



# Structural, Morphological and Electrical Impedance Spectroscopy of $\text{Bi}_2\text{MnCdO}_6$ Double Perovskite Electronic Material

A. Tripathy<sup>1</sup> · S. N. Das<sup>1</sup> · S. Bhuyan<sup>1</sup> · R. N. P. Choudhary<sup>1</sup>

Received: 9 December 2018 / Revised: 2 March 2019 / Accepted: 28 March 2019 / Published online: 3 April 2019  
© The Korean Institute of Electrical and Electronic Material Engineers 2019

## Abstract

In this communication, the systematic studies of structural (basic crystal data, microstructure), and electrical (dielectric constant and loss, impedance, modulus, conductivity, etc.) properties of the double perovskite material  $\text{Bi}_2\text{MnCdO}_6$  have been reported. The compound has been synthesized by means of a high temperature route (a solid state reaction method). From the X-ray diffraction structural investigation, a stable phase of the orthorhombic crystal system has been recognized. The microstructure obtained from the scanning electron microscope shows uniform, dense and compact grain distribution. Detailed investigation of dielectric as well as electrical parameters of the fabricated compound through a broad frequency range (i.e. 1 kHz–1 MHz) and temperature (i.e., 25 °C to 300 °C) have provided many interesting data and results in order to understand its ferroelectric and electrical relaxation mechanism. It has been experimentally affirm that this material ( $\text{Bi}_2\text{MnCdO}_6$ ) has more advantages like high relative dielectric constant and low tangent loss over  $\text{Bi}_2\text{MnCoO}_6$  material.

**Keywords** Double perovskite · Dielectric · Electronic material

## 1 Introduction

Double perovskites (DPs) materials have a gigantic potential for application in the fields of electronic devices, sensors, microwave technologies, magnetic memory components, components for solar cells, fuel cell superconductors, micro-electronics mechanical systems etc. [1–6]. They exhibit different properties such as insulating, metallic, ferromagnetic, magneto-dielectric, multiferroic, etc. [7–9]. Perovskites are commonly crystalline class of materials with  $\text{ABX}_3$  structure which resembles  $\text{CaTiO}_3$  structure. They are now-a-days generally found in various compounds. They can also be in many different new material combinations either in simple or complex crystal structure. But they have certain limitations basically because of their (1) toxicity and probable carcinogenicity (due to the presence of lead and lead halides mostly), and (2) chemical instability (especially its inclination towards light, humidity and air. The most broadly studied and efficient perovskite materials are based on  $\text{ABX}_3$

structure, where A and B are the monovalent cation and divalent cation respectively, and the X-site of the structure is engaged by the counter anionic species such as oxide ( $\text{O}^{2-}$ ) and non-oxide perovskite like halides ( $\text{Cl}^-$ ,  $\text{Br}^-$  and  $\text{I}^-$ ) and chalcogenide ( $\text{S}^{2-}$ ,  $\text{Se}^{2-}$  and  $\text{Te}^{2-}$ ) etc. By interchanging the positions of A-site, B-site or X-site ions, these perovskites properties can be altered which can give an excellent result to evaluate performance of the perovskites for many electronics devices and other applications. Further, by substituting suitable metal cations B and B' (transition metals) as well as the alkali, alkaline, post transition or rare earth ions A within their distinctive tolerance limit, the perovskite properties can be modified to provide double perovskite structure (a common formula  $\text{A}_2\text{BB}'\text{O}_6$ , show rock-salt like structural arrangement, where the corner-sharing units  $\text{BO}_6$  and  $\text{B}'\text{O}_6$  of the structure are the versatile lucrative set of compounds) to realize an additional degree of freedom along with the fine tuning of its cation ordering, dielectric and electrical properties [10–14]. Due to the difference in ionic radii or/and oxidation states of B and B' cations, these double perovskites often shows the inclination towards cation ordering and half metallic properties. Also the co-existence of delocalized and bound electrons adds up these characteristics [15, 16]. Prior work also suggests and confirms the formation of DPs structures. There are different methods for

✉ S. Bhuyan  
satyanarayanbhuyan@soa.ac.in

<sup>1</sup> Department of Electronics and Communication Engineering, Siksha 'O' Anusandhan (Deemed to be University), Bhubaneswar 751030, India

synthesis of DP ceramic materials like the one step thermal decomposition method and solid state reaction method [17]. The dielectric properties have been extensively investigated for most of the DP materials. The existence of ferro-electricity in these materials (A position mostly occupied by materials like Bi, La, Lu, Dy etc. and B position has been substituted with Ni and Co—a combination of rare earth and transition metals) has already been proved [15, 16]. The exciting dielectric features create a honker wave among the researchers to continue their research in the field of double perovskites. Owing to its significance, the bismuth allied novel  $\text{Bi}_2\text{MnCdO}_6$  double perovskite electronic material has been chosen. In the double perovskite arrangement of  $\text{Bi}_2\text{MnCdO}_6$  (A, B, B' site contains  $\text{Bi}^{+3}$ ,  $\text{Mn}^{+4}$  and  $\text{Cd}^{+2}$  cations respectively) where Mn has partially filled and Cd has empty orbital's or vice versa arrangement takes place, which provides unique multiferroic behavior due to their ferromagnetic insulator behaviors which has  $180^\circ$  super exchange interaction between B and B' cation via oxygen ions. In this present work, the desired oxide compound  $\text{Bi}_2\text{MnCdO}_6$  has been formulated and synthesized via the solid state reaction path at a high temperature. An extensive assessment has been conducted to showcase its morphological, structural, dielectric and electrical performance in a direction towards the electronic device applications.

## 2 Experimental Procedure

The double perovskite sample of  $\text{Bi}_2\text{MnCdO}_6$  has been prepared at high temperature (nearly  $600^\circ\text{C}$ ) by the regular solid state reaction method with the help of analytical grade or high purity ( $>99.9\%$ )  $\text{Bi}_2\text{O}_3$ ,  $\text{CdO}$ ,  $\text{MnO}_2$ . All these oxides with their required stoichiometric ratios (in order to compensate bismuth loss and maintain desired stoichiometric after processing, 2% extra bismuth oxide is taken) are mixed thoroughly by dry grinding in the air medium (using agate pestle and mortar) trailed by wet grinding in the presence of volatile methanol medium till its evaporation in-order to obtain a uniform/homogeneous mixture. Then obtained homogeneously mixed fine powder is calcined at a temperature of  $600^\circ\text{C}$  in an aluminum crucible for 4 h. The high temperature of the furnace is achieved in a stepwise manner through a microcontroller controlled program. Then, the formation of the chosen compound has been established through X-ray diffraction (XRD) method by using X-ray powder diffractometer ( $\lambda = 1.5405 \text{ \AA}$ ) in a large range of Bragg angle  $\theta$  ( $20^\circ < 2\theta < 80^\circ$ ) at a scanning speed of  $2^\circ/\text{min}$ . Then the calcined powder of the compound has been thoroughly mixed with a drop of polyvinyl alcohol (PVA) which is used for granulation purpose and then compact cylindrical pellet samples of 12 mm in diameter and 1–2 mm in thickness is obtained by pressing it through

a uniaxial hydraulic press under a pressure of  $4 \times 10^6 \text{ N/m}^2$ . Then these pellets are sintered on an aluminum boat at  $630^\circ\text{C}$ . Here, the temperature is increased gradually in a controlled manner so that the PVA is evaporated completely minimizing the creation of voids in the samples. Finally, we obtained compact and dense cylindrical pellets for further characterization. The micrographs of the sample are then recorded and examined through a scanning electron microscope (SEM—Model ZEISS). A pellet is then coated with analytical grade silver paste which acts as electrodes (heated at  $100^\circ\text{C}$  for 1 h) for a further electrical measurement. By using a phase-sensitive analyzer (N4L PSM1735), various parameters such as the relative permittivity, impedance, capacitance, etc., are obtained as a function of temperature (through  $25^\circ\text{C}$  to  $300^\circ\text{C}$ ) over a range of frequency varies from 1 kHz–1 MHz. Laboratory-fabricated sample holders along with vertical pit furnace have been procured in our followed experimental set up to control the variation of temperature. To record the temperatures inside the sample holder which is assumed to be the temperature of sample surroundings, a chromel–alumel thermocouple and a digital millivoltmeter (RISH MULTI 15S) is used.

## 3 Results and Analysis

### 3.1 Structural and Morphological Characteristics

The room temperature XRD of individual powder compounds and the formation of new double perovskite compound have been carried out and their XRD pattern have been depicted in Fig. 1. By comparing with the standard X-ray diffraction data file (JCPDS 76-1730, JCPDS 44-141 and JCPDS-05-0640 respectively) it has been seen that the obtained results of individual compounds are similar to those of the peaks of the basic ingredients. The major peaks of the desired compound  $\text{Bi}_2\text{MnCdO}_6$  are equivalent to the double perovskite structure, but dissimilar from those of the basic ingredients, and thus ascertaining the formation of a different compound. With the help of POWD software (a standardized computer program package), and by taking into account the acquired  $2\theta$  values of the diffraction pattern the major peaks are indexed [18]. An excellent concurrence between the calculated (cal.) and observed (obs.) inter-planar positioning  $d$  (i.e.,  $\sum \Delta d = d_{obs} - d_{cal} = \text{minimum}$ ) is obtained. Using the refined values of inter-planar distance, lattice parameters and other structural parameters, each peak has carefully been indexed. The formation of the monoclinic crystal system has been selected for synthesized compound by considering the several factors, including the least standard deviation (LSD), and the best agreement of the experimental and calculated parameters [19, 20]. The structural

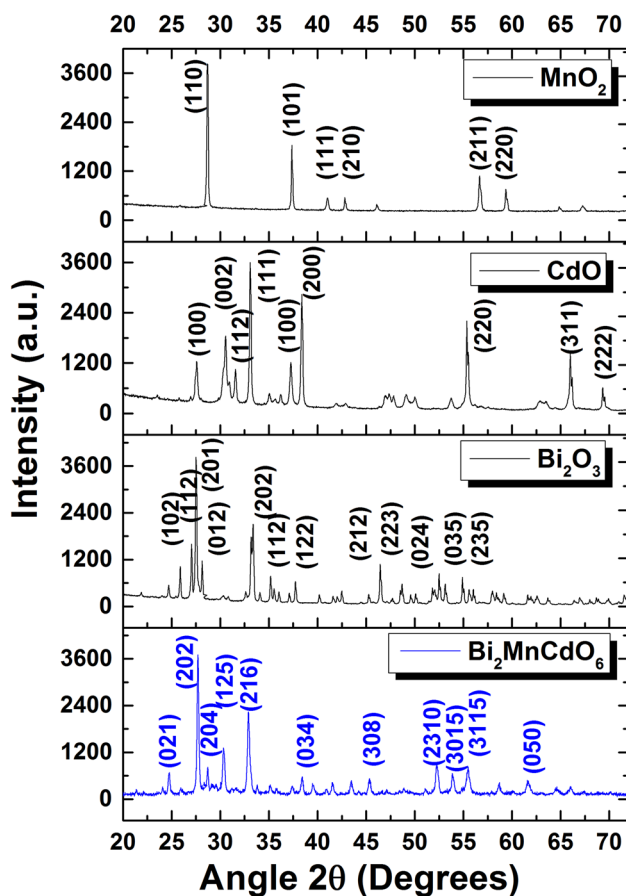


Fig. 1 Room temperature XRD pattern of  $\text{Bi}_2\text{O}_3$ ,  $\text{MnO}_2$ ,  $\text{CdO}$  and  $\text{Bi}_2\text{MnCdO}_6$

parameters and the Miller Indices (hkl) of the synthesized material are nearly equal to the double perovskite compounds. The best fitted lattice parameters of the prepared compound are as follows:  $a = 6.4515(36) \text{ \AA}$ ,  $b = 7.1796(36) \text{ \AA}$ ,  $c = 6.2270(36) \text{ \AA}$ , (the inside the parenthesis is the estimated standard deviation in the lattice parameters),  $\beta = 94.06^\circ$  and  $V = 287.71 (\text{ \AA})^3$  with a standard deviation of  $SD = 0.0036$ . These lattice dimensions are consistent and comparable with most of the distorted double perovskite materials. Above lattice dimension is somehow larger as compared to that of some rare-earth (R) based double perovskite ( $\text{R}_2\text{NiMnO}_6$ ) because of the difference in the atomic size of the elements of the compound. The detailed X-ray analysis ascertains the development of a novel and stable single phase monoclinic crystal system.

The scanning electron micrograph (SEM) of the sintered pellet of  $\text{Bi}_2\text{MnCdO}_6$  has been depicted in Fig. 2. A dense and compact grain distribution of different shape and size has been observed on the pellet surface. For proper electrical measurements the uniform distribution of the grains without any void is the necessary condition,

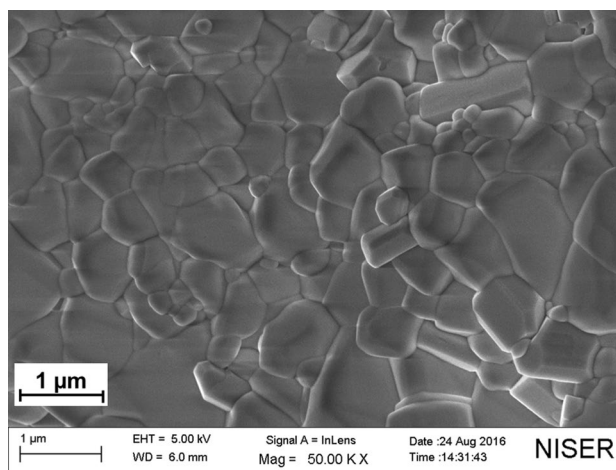


Fig. 2 Room temperature SEM micrograph of  $\text{Bi}_2\text{MnCdO}_6$

and that can be checked from the micrographs. The average size of the grains is estimated to be  $0.2\text{--}0.6 \mu\text{m}$ .

The elemental composition study of the developed material has been carried out through EDX (energy dispersive X-ray) analysis. The obtained energy dispersive spectra have been depicted in Fig. 3. It is observed that there is no impurity content and the peaks are showing the presence of elements Bi, Mn, Cd and O. Hence, from the EDX analyzer it is affirmed that the synthesized compound and the samples mixed with their stoichiometric compositions resemble each other closely.

### 3.2 Dielectric Properties

The temperature dependence of  $\epsilon_r$  (relative dielectric constant) and  $\tan \delta$  (tangent loss) of the compound  $\text{Bi}_2\text{MnCdO}_6$  at different selected frequencies has been depicted in Fig. 4. Two most important factors of dielectric materials are tangent loss ( $\tan \delta$ ) and relative dielectric constant ( $\epsilon_r$ ).  $\epsilon_r$  informs about the amount of energy stored in a material and  $\tan \delta$  informs about the amount of energy loss. The relative

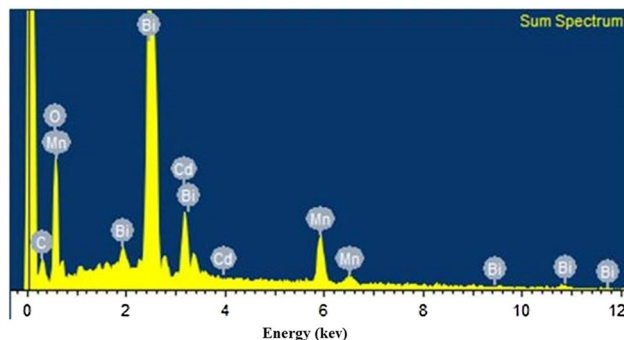
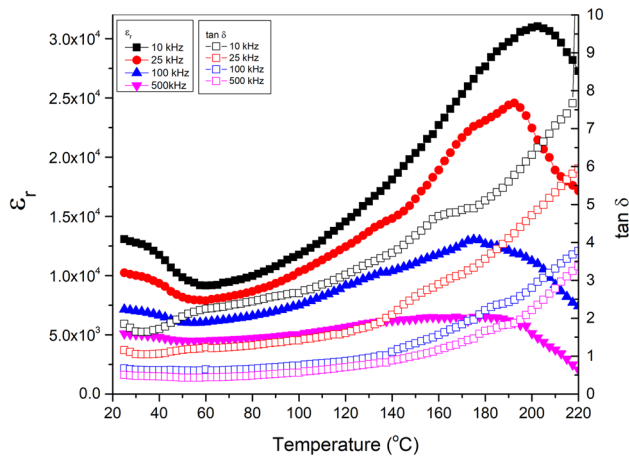
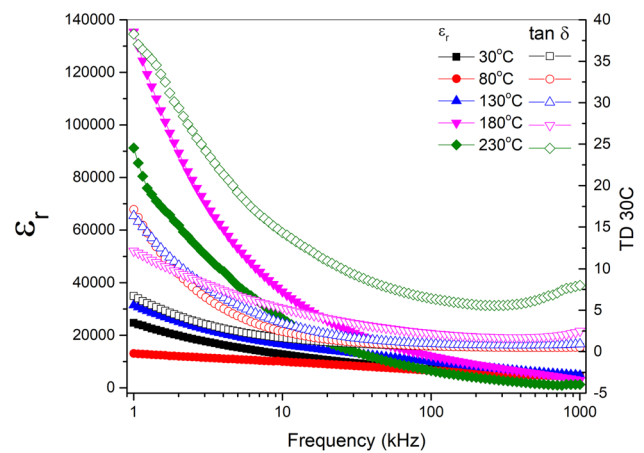


Fig. 3 Measured composition EDAX graphs of  $\text{Bi}_2\text{MnCdO}_6$



**Fig. 4** Temperature dependence of dielectric constant and tangent loss at selected frequencies of  $\text{Bi}_2\text{MnCdO}_6$

dielectric constant is mostly linked with electronic, atomic and dipolar polarization effects of the material which are under the effect of ac fields. The relative dielectric constant declines with rise of temperature and attends minima and afterwards the value rises to attend a prominent maxima peak (at  $\sim 200^\circ\text{C}$ ) is observed. The peak which is seen at higher temperature moves towards lower temperature well marked peak broadening as well as diffusive phase transition is observed which signifies the relax or behavior of the compound at higher temperature. For this material it can be assorted that at different selected frequencies like 10, 100, 500 kHz the phase transition temperature values are 200, 175, 160  $^\circ\text{C}$  respectively, which shows that the decline in phase transition temperature with the rise of frequency. But for the  $\text{Bi}_2\text{MnCoO}_6$  ceramic material for the same frequencies the phase transition temperature values are 140, 160 and 180  $^\circ\text{C}$  respectively. Also it shows that as frequency value increases the phase transition temperature values decreases. Similarly the tangent loss has also surged with the rise in temperature. The scattering of thermally triggered charge carriers and transient interaction between the cations ( $\text{Bi}^{3+}$ ,  $\text{Mn}^{3+}$ ,  $\text{Co}^{3+}$ ) with oxygen vacancies may be responsible for a rise in tangent loss at elevated temperature. Simultaneously with the rise of frequency the tangent loss declines. For this material the values of tangent loss at selected frequencies like 10, 100, 500 kHz are nearly 10, 4, 3.5 respectively, whereas for the  $\text{Bi}_2\text{MnCoO}_6$  ceramic material at the same frequencies, the values are comparatively high nearly 130, 30, 20 respectively. But the pattern of tangent loss is similar for both the materials. As the tangent loss is low for this material it can say that this material is much better as compared to that of the previously reported material. Recently, Das et al. [21] have reported some interesting work on double perovskite material, and compared to their material, this



**Fig. 5** Frequency dependence of dielectric constant and tangent loss at specific temperatures of  $\text{Bi}_2\text{MnCdO}_6$

material has high relative dielectric constant and low tan delta values.

The frequency reliance of dielectric constant ( $\epsilon_r$ ) and loss tangent ( $\tan \delta$ ) of the fabricated compound at some of the particular temperature values is shown in Fig. 5. Both of the factors are decreasing with an increase in frequencies which is a property of the general dielectric materials [22–25]. The increase in dielectric constant with a decrease in frequency is due to the contribution from different kinds of polarization effects such as interfacial, atomic, ionic, dipolar, and electronic polarizations, and charge accumulation at the boundary. But at higher frequencies, lack of charge build-up at the interfaces results in an invariant dielectric constant. To summarize, with the increase in frequency at particular chosen temperatures of 30  $^\circ\text{C}$ , 80  $^\circ\text{C}$ , 130  $^\circ\text{C}$ , 180  $^\circ\text{C}$ , 230  $^\circ\text{C}$  and 280  $^\circ\text{C}$ , the relative dielectric constant are nearly (2.2, 1.5, 3.2, 13.7, 9.6, 5)  $\times 10^4$  respectively which is high for this material. Similarly for the  $\text{Bi}_2\text{MnCoO}_6$  ceramic material at the chosen temperatures 30  $^\circ\text{C}$ , 80  $^\circ\text{C}$ , 130  $^\circ\text{C}$  and 180  $^\circ\text{C}$ , the corresponding values of  $\epsilon_r$  are 1100, 1700, 2200, and 1800 respectively. But both the graphs follow the same pattern. Similarly, with increasing frequency at selected temperatures like 30  $^\circ\text{C}$ , 80  $^\circ\text{C}$ , 130  $^\circ\text{C}$ , 180  $^\circ\text{C}$ , 230  $^\circ\text{C}$  and 280  $^\circ\text{C}$ , the value of tangent loss is found to be nearly 8, 17, 15, 13, 38 and 33 which is comparatively lower for this material as compared with the values of the  $\text{Bi}_2\text{MnCoO}_6$  ceramic material. Similarly, for the  $\text{Bi}_2\text{MnCoO}_6$  ceramic material at the selected temperature 30  $^\circ\text{C}$ , 80  $^\circ\text{C}$ , 130  $^\circ\text{C}$  and 180  $^\circ\text{C}$ , the corresponding values of  $\tan \delta$  are 10, 30, 130 and 190 respectively. The studied material can withstand higher temperature (up-to 300  $^\circ\text{C}$ ) as compared to that of previously reported material (up-to 200  $^\circ\text{C}$  after which again phase transition takes place). So, the prepared material may be suitable for higher temperature applications.

### 3.3 DC Conductivity Study

Figure 6 depicts the I–V (DC current vs voltage) characteristics of the developed compound over a broad range of temperature (25 °C to 150 °C). It is useful in-order to gather data about leakage current. Generally, the DC current here is increasing non-linearly with increases in both electric voltage and temperature [26–28]. This nature of variation is in accordance with the behavior of the semiconductor materials. After a definite point of temperature the DC value of current reaches a maxima and thereafter remains constant. It is because of the saturation of the ions responsible for conduction process.

### 3.4 AC Conductivity Study

The inverse of absolute temperature reliance of AC conductivity ( $\sigma_{AC}$ ) at few selected frequency values are depicted in Fig. 7, and the frequency dependence at selected temperature values are shown in Fig. 8. Activation energy ( $E_a$ ) as well as conductivity values have been calculated and with the help of following mathematical expressions through the linear fitting to Arrhenius plots [29–31].

$$\sigma_{AC} = \omega \epsilon \epsilon_0 \tan \delta \tag{1}$$

$$\sigma_{AC} = \sigma_0 \exp(-E_a/kT) \tag{2}$$

Different slopes are obtained in the high temperature regions for different selected frequencies. The activation energy has been calculated from the temperature dependent conductivity, and the values are found to be 0.46, 0.39, 0.33 and 0.28 eV at 1, 10, 100 and 500 kHz frequency respectively. For every frequency in the plot, there exists dissimilar slope in the certain temperature region. This advocates the

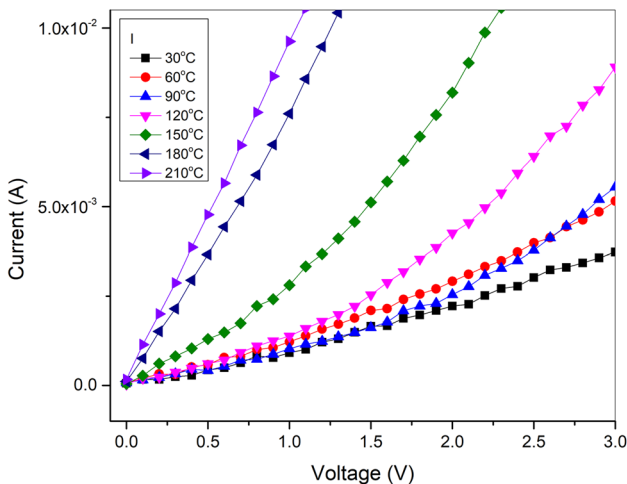


Fig. 6 I–V characteristic of the compound  $\text{Bi}_2\text{MnCdO}_6$

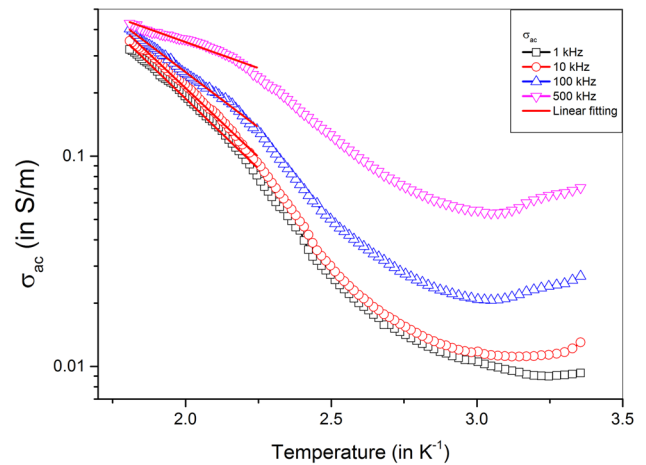


Fig. 7 Temperature dependent AC conductivity spectrum at selected frequency of  $\text{Bi}_2\text{MnCdO}_6$

occurrence of several conduction phenomena in the compound with multiple activation energies.

In the conductivity spectrum, it can be seen that at low frequency, the rate of rise in conductivity is slower as compared to that of high frequency. With an increase in temperature, the conductivity also increases. The frequency dependence of AC conductivity is fitted through non-linear curve fitting method using the Jonscher’s power law [32]. It is given as below:

$$\sigma_{AC} = \sigma_{DC} + A\omega^n \tag{3}$$

where  $\sigma_{AC}$  is the AC conductivity,  $\sigma_{DC}$  is the DC conductivity at lower frequencies and at selected temperatures, A is a constant, and the exponent n lies between  $0 < n < 1$ . We can see that the conductivity proliferates with frequency. A

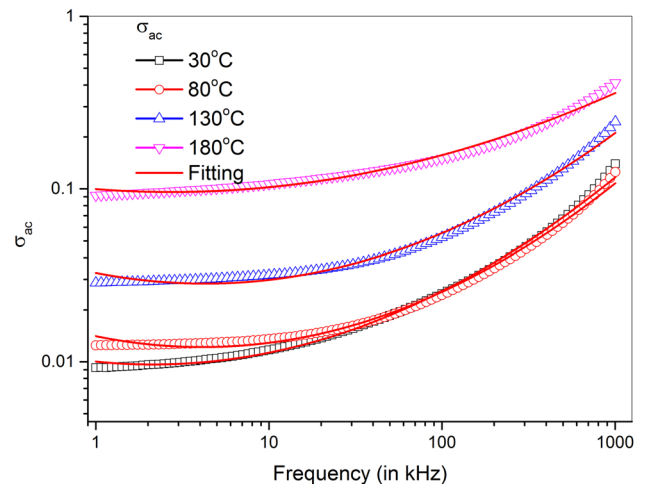


Fig. 8 Frequency dependent AC conductivity spectrum at selected temperature of  $\text{Bi}_2\text{MnCdO}_6$

flat response is obtained at lower frequency and at higher temperature regions. This behavior is basically because of the polarization consequence at the electrode and dielectric boundary. As the frequency increases, the build-up charge reduces, resulting in an increase in the conductivity values.

### 3.5 Impedance Spectrum

Complex impedance spectroscopy (CIS) is a valuable tool which is used to examine the electrical properties and the related conduction process of the material which depends upon the grain, grain boundaries and electrode effects. In CIS the dielectric properties of a material are measured in terms of the frequency. The CIS technique is the AC response analysis of a pre-defined system through application of a sinusoidal signal and successive estimation of its impedance as well as its allied parameters as a function of frequency and temperatures. Impedance parameters of materials such as resistive, capacitive and constant phase components are generally represented by the Nyquist plot which forms successive semicircles. The dielectric spectrum characteristics of the materials are normally explained in terms of complex parameters.

The variations of both the parameters [real ( $Z'$ ) and imaginary ( $Z''$ ) part of the impedance] of the impedance spectroscopy at particular temperature values are given in Fig. 9. The value of  $Z'$  displays a decreasing trend with an escalation in frequency. A peak of a particular frequency value is observed with a shifting of peak towards the higher frequency region with the elevation of temperature. For this material, the values of  $Z'$  at certain selected temperatures like 30 °C, 80 °C, 130 °C, 180 °C, 230 °C and 280 °C is found to be 2, 1.5, 0.7, 0.4, 0.3 and 0.1 kΩ. But for the similar material  $\text{Bi}_2\text{MnCoO}_6$ , the values of  $Z'$  at a certain temperature like 30 °C, 80 °C, 130 °C, 180 °C, the such

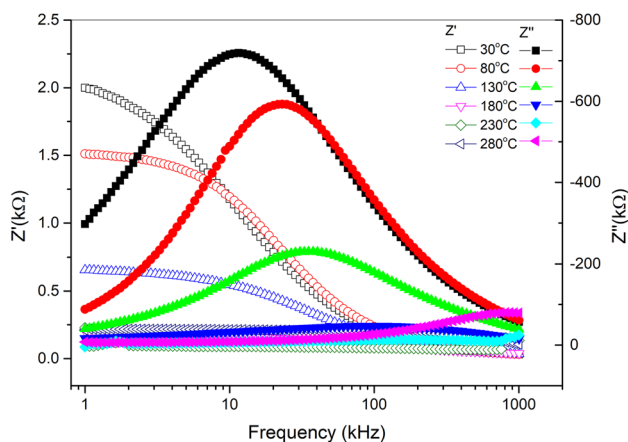


Fig. 9 Frequency dependence complex impedance properties at selected temperatures of  $\text{Bi}_2\text{MnCdO}_6$

value is 45, 9, 3 and 2 kΩ respectively. This shows that the resistance of the studied material is lower as compared to the previous material. The  $Z''$  graph also shows the peak at certain frequency values and gradually becomes flat with an increase in temperature, i.e., at the high temperature peaks are broader in comparison to the low temperature-peak.

The Nyquist plot (complex impedance spectrum) of the material has been depicted in Fig. 10 obtained at some selected temperature values through a broad choice of frequency values (between 1 kHz and 1 MHz). The real part of the impedance is reflected in X-axis, while the imaginary part in the Y-axis. Each individual point in the semicircle represents the impedance of a particular frequency. Here with the escalation of temperature the radius of the semicircle reduces and also the formation of semicircular tendency increases [33]. Instead of perfect semicircle depressed semicircle is observed which suggest its non-Debye type characteristics. By using a computer controlled circuit model software (Z-win software version 2.0) the experimentally acquired physical readings are fitted with simulated circuit model data's. The fitted electrical circuit proto-type includes a parallel connection of circuit elements  $C_b$  and  $R_b$  which is further connected in series with the parallel combination of  $R_{gb}$ , CPE and  $C_{gb}$  (where  $C_b$ =bulk capacitance,  $R_b$ =bulk resistance,  $R_{gb}$ =grain resistance, CPE=constant phase element and  $C_{gb}$ =grain capacitance respectively) as depicted in Fig. 10. The simulated parameter values obtained for selected temperatures are represented in the Table 1.

### 3.6 Complex Electric Modulus Analysis

Figure 11 depicts the dependency of  $M'$  and  $M''$  with frequency at nominated temperatures. At lower temperature the value of  $M'$  shows a peak at a lower frequency and then

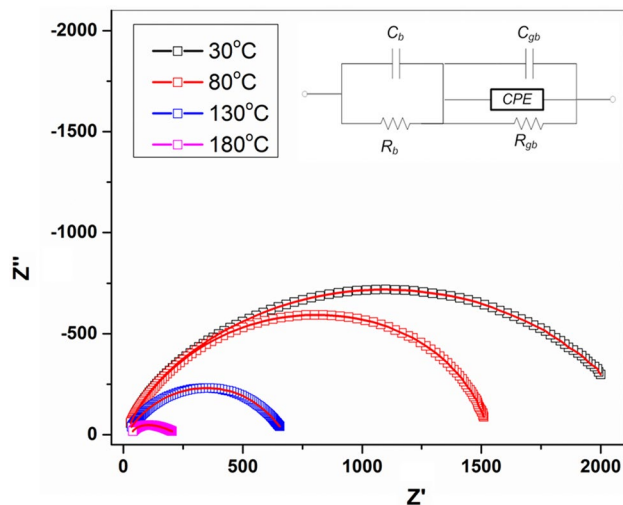
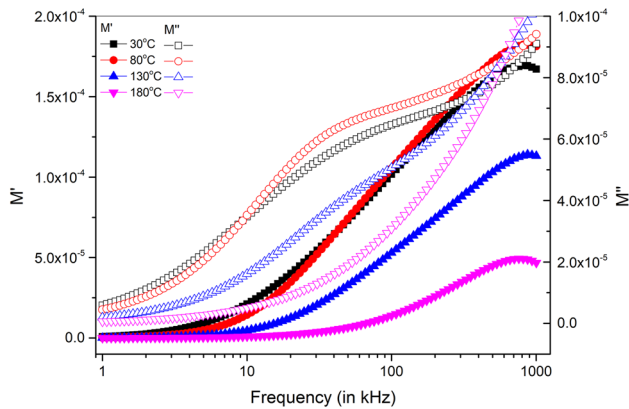


Fig. 10 Nyquist plot of  $\text{Bi}_2\text{MnCdO}_6$

**Table 1** Simulated fitting parameters of bulk and grain boundary resistance as well as capacitance of the compound  $\text{Bi}_2\text{MnCdO}_6$

Temperature	$R_b$ ( $\Omega$ )	$C_b$ (F)	$R_{gb}$ ( $\Omega$ )	CPE	$C_{gb}$ (F)
30 °C	$4.25 \times 10^5$	$1.53 \times 10^{-7}$	$2.32 \times 10^4$	$6.59 \times 10^{-8}$	$9.56 \times 10^{-11}$
80 °C	$5.29 \times 10^4$	$2.25 \times 10^{-7}$	$5.23 \times 10^3$	$6.78 \times 10^{-8}$	$9.12 \times 10^{-10}$
130 °C	$2.41 \times 10^4$	$1.26 \times 10^{-6}$	$1.07 \times 10^2$	$7.12 \times 10^{-8}$	$2.82 \times 10^{-10}$
180 °C	$4.22 \times 10^2$	$6.11 \times 10^{-6}$	$2.72 \times 10^3$	$9.56 \times 10^{-8}$	$1.44 \times 10^{-10}$



**Fig. 11** Electrical modulus spectrum of  $\text{Bi}_2\text{MnCdO}_6$

approaches to zero which may be due to the thermally activated relaxation phenomena [34, 35]. The higher temperature graphs don't show any variation with an increase in the frequency. The same result is being obtained with the  $M''$  graph. The following relations of electrical modulus has been utilised for estimation of  $M'$  and  $M''$  values:

$$M' = A \left[ \frac{(\omega RC)^2}{1 + (\omega RC)^2} \right] = A \left[ \frac{\omega^2 \tau^2}{1 + \omega^2 \tau^2} \right] \quad (4)$$

$$M'' = A \left[ \frac{\omega RC}{1 + (\omega RC)^2} \right] = A \left[ \frac{\omega \tau}{1 + \omega^2 \tau^2} \right] \quad (5)$$

where  $A = \frac{C_0}{C}$ .

## 4 Conclusion

The double perovskite sample of  $\text{Bi}_2\text{MnCdO}_6$  has been prepared at high temperature by the regular solid state reaction method. The structure, grain distribution as well as electrical properties have been explored as a function of both temperature and frequency. The detailed X-ray analysis ascertains the development of a novel and stable single phase monoclinic crystal system. A dense and compact grain distribution of different shape and size has been observed from SEM analysis. EDX analysis suggests that the synthesized compound and the samples mixed with their stoichiometric compositions resemble each other closely. The

temperature dependence of  $\epsilon_r$  (relative dielectric constant) and  $\tan \delta$  (tangent loss) of the compound  $\text{Bi}_2\text{MnCdO}_6$  at different selected frequencies has been analyzed. It shows that as frequency value increases the phase transition temperature values decreases. Simultaneously with the rise of frequency the tangent loss declines. As the tangent loss is low and dielectric constant is high for this material, so it can urge that this material is much better as compared to that of the previously reported material. The impedance study confirms the semiconductor characteristics at high temperature (negative temperature coefficient of resistance-NTCR). A typical non-Debye type relaxation phenomenon has been observed from the impedance analysis. The obtained useful information may be very much useful towards the development of electronic devices.

## References

1. W. Eerenstein, N.D. Mathur, J.F. Scott, *Nat. Lond.* **442**, 759 (2006)
2. Y. Lan, X. Feng, X. Zhang, Y. Shen, D. Wang, *Phys. Lett. A* **380**, 2962 (2016)
3. A.K. Paul, M. Reehuis, V. Ksenofontov, B.H. Yan, A. Hoser, D.M. Töbrens, P.M. Abdala, P. Adler, M. Jansen, C. Felser, *Phys. Rev. Lett.* **111**, 1 (2013)
4. M. Green, A.H. Baillie, H.J. Snaith, *Nat. Photonics* **8**, 506 (2014)
5. G. Volonakis, M.R. Filip, A.A. Haghighirad, N. Sakai, B. Wenger, H.J. Snaith, F. Giustino, *J. Phys. Chem. Lett.* **7**, 1254 (2016)
6. A.H. Slavney, T. Hu, A.M. Lindenberg, H.I. Karunadasa, *J. Am. Chem. Soc.* **138**, 2138 (2016)
7. L. Luo, L. Zhou, X. Zou, Q. Zheng, D. Lin, *J. Mater. Sci. Mater. Electron.* **25**, 4896–4901 (2014)
8. M.M. Kumar, V.R. Palkar, K. Srinivas, S.V. Suryanarayana, *Appl. Phys. Lett.* **76**, 2764 (2000)
9. S.N. Das, S.K. Pradhan, D.P. Kar, S. Bhuyan, R.N.P. Choudhary, *J. Mater. Sci. Mater. Electron.* **29**, 9375 (2018)
10. A. Tripathy, S.N. Das, S.K. Pradhan, S. Bhuyan, R.N.P. Choudhary, *J. Mater. Sci. Mater. Electron.* **29**, 4770 (2018)
11. H.J. Feng, F.M. Liu, *Phys. Lett. A* **372**, 1904 (2008)
12. Y.Q. Lin, X.M. Chen, *J. Am. Ceram. Soc.* **94**(3), 782–787 (2011). **DPS**
13. M. Ullah, S.A. Khan, G. Murtaza, R. Khenata, N. Ullah, *J. Magn. Magn. Mater.* **377**, 197–203 (2015). **DPS**
14. O.E. Rhazouani, A. Slassi, Y. Ziat, A. Benyoussef, *Phys. Lett. A* **381**, 1177 (2017)
15. C.L. Bull, D. Gleeson, K.S. Knight, *J. Phys. Condens. Matter* **15**, 4927 (2003)
16. M. Azuma, K. Takata, T. Saito, S. Ishiwata, Y. Shimakawa, M. Takano, *J. Am. Chem. Soc.* **127**, 8889 (2005)

17. T. Siritanon, N. Chathirat, C. Masingboon, T. Yamwong, S. Maensiri, *J. Mater. Sci. Mater. Electron.* **25**, 1361–1868 (2014)
18. E. Wu, *J. Appl. Cryst.* **22**, 506 (1989)
19. B.D. Cullity, *Elements of X-ray Diffraction* (Addison-Wesley, Reading, 1978)
20. B. Asbani, A. Lahmar, M. Amjoud, J.L. Dellis, Y. Gagou, D. Mezzane, M.E. Marssi, *Superlattices Microstruct.* **71**, 162 (2014)
21. R. Das, R.N.P. Choudhary, *Solid State Sci.* **87**, 1–8 (2019)
22. S.K. Pradhan, S.N. Das, S. Halder, S. Bhuyan, R.N.P. Choudhary, *J. Mater. Sci. Mater. Electron.* **28**, 9627 (2007)
23. K.K. Mishra, A.T. Satya, A. Bharathi, V. Sivasubramanian, V.R.K. Murthy, A.K. Arora, *J. Appl. Phys.* **110**, 123529 (2011)
24. S.N. Das, A. Pattanaik, S. Kadambini, S. Pradhan, S. Bhuyan, R.N.P. Choudhary, *J. Mater. Sci. Mater. Electron.* **27**, 10099 (2016)
25. S.N. Das, S.K. Pradhan, S. Bhuyan, S. Sahoo, R.N.P. Choudhary, M.N. Goswami, *J. Electron. Mater.* **47**, 843 (2017)
26. D.K. Pradhan, B. Behera, P.R. Das, *J. Mater. Sci. Mater. Electron.* **23**, 779 (2012)
27. W. Liu, G. Tan, G. Dong, X. Xue, H. Ren, A. Xia, *Superlattices Microstruct.* **72**, 186 (2014)
28. V. Provenzano, L.P. Boesch, V. Volterra, C.T. Moynihan, P.B. Macedo, *J. Am. Ceram. Soc.* **55**, 492 (1972)
29. H. Jain, C.H. Hsieh, *J. Solids Non Cryst.* **172**, 1408 (1994)
30. D.P. Almond, A.R. West, *Solid State Ion.* **11**, 57 (1983)
31. S. Chatterjee, P.K. Mahapatra, R.N.P. Choudhary, A.K. Thakur, *Phys. Stat. Sol. (a)* **201**, 588 (2004)
32. S.N. Das, S. Pradhan, S. Bhuyan, R.N.P. Choudhary, P. Das, *J. Electron. Mater.* **46**, 1637 (2016)
33. C.K. Suman, K. Prasad, R.N.P. Choudhary, *J. Mater. Sci.* **41**, 369 (2006)
34. Y. Zhang, J.P. Zhou, Q. Liu, S. Zhang, C.Y. Deng, *Ceram. Int.* **40**, 5853 (2014)
35. R. Mukherjee, A. Dutta, T.P. Sinha, *J. Electron. Mater.* **45**, 846 (2016)

**Publisher's Note** Springer Nature remains neutral with regard to jurisdictional claims in published maps and institutional affiliations.